Cement and Concrete Research 40 (2010) 997–1008

Contents lists available at ScienceDirect

Cement and Concrete Research

journal homepage: http://ees.elsevier.com/CEMCON/default.asp

Early-age behavior of materials with a cement matrix

J.F. Georgin *, T. Le Bihan, J. Ambroise, J. Pera

Laboratory LGCIE, INSA LYON, Villeurbanne 69621, France

ARTICLE INFO

Article history:
Received 1 July 2009
Accepted 10 March 2010

Keywords:
Cement material (D)
Screed
Shrinkage (C)
Pore pressure
Pore-size distribution (B)

ABSTRACT

Materials with a cement matrix classically present early-age volume variations (shrinkage and/or swelling). This intrinsic early-age behavior strongly influences the length of time the buildings and structures will last because of the micro-cracking and cracking that results from it. One explanation for the macroscopic shrinkage is the presence of pore pressure in the porous medium. In this study, fine modeling of the coupling mechanism behind these internal strains is proposed. The chemical reaction associated with hydration is considered as the main force behind the hydric and mechanical evolutions in an endogenous configuration. Thus, the influence of chemical contraction, porosity, pore-size distribution and pore pressure are central to the study in the light of the numerical and experimental results obtained. A self-leveling layer of mortar of sulfo-aluminous concrete base was used.

1. Introduction

With a view to answering the needs of society, for example in terms of reducing CO_2 emissions and saving energy, the use of strongly aluminous-based cements is advantageous. For example, the rapid hydration kinetics of these cements brings gains in productivity and saves energy at the prefabrication stage. Similarly, obtaining these cements at lower temperatures than those required for Portland cements leads to lower CO_2 emissions per ton of cement produced. Moreover, the less important quantity of calcium inside raw materials leads also to decrease CO_2 emissions during industrial clinker making process. Besides, concerning problems of material durability, knowledge of the early-age behavior of materials with a cement matrix is a major stake in the development of these new binders. Indeed, like all materials with a cement matrix, they unfortunately show considerable early-age volume variations. This can be due to shrinkage or swelling imposed by hydration conditions and the thermic and hydric environment. The use of sulfo-aluminous cement [1] in the making of self-leveling concrete screeds seems to have a considerable advantage compared to the use of Portland cements [2] concerning screeds curling and cracking problems. The very nature of the hydrates formed is such that the pore-size distribution includes pore families of higher radius than in Portland cements and C–S–H gel. The reduction in the degree of saturation in the porous networks inherent in hydration leads to the creation of menisci which cause capillary pressure. The existence of pore pressure thus leads to skeleton contraction and macroscopic shrinkage. From an experimental point of view, it remains very difficult to isolate precisely the cause and effect relationship between the macroscopic observations and the material characteristics for the chemical, hydric, thermic and mechanical mechanisms are closely linked. A fine modeling approach is also needed as a complementary tool to experimentation for studying the coupling aspects which influence the amplitude of volume variations observed at an early age.

In this paper, the equations governing the chemical, hydric and mechanical behavior of a porous material at an early age are proposed. The thermic aspect which certainly plays a role, will not be treated here. The modeling parameters are identified using the results of the measurement of the degree of hydration, the pore-size distribution and loss mass of a drying screed. The capacity of the model is first evaluated in an endogenous configuration, that is, without taking into consideration the drying mechanism, by confronting the calculated internal pore pressure and the pore pressure measured experimentally. Then the analysis will be extended to the drying of a concrete screed exposed to 50% relative humidity on its upper side. The representativeness of the numerical approach will then be evaluated globally from the mass loss. The main objective of this paper is not to validate the proposed numerical model because it requires more work which will be presented in subsequent publications. The aim is essentially to show all the potential of the proposed modeling of the pore-size distribution at an early age permitting to simulate the mass transfer in material during the first hours or days after casting.

2. Modeling approach

2.1. Hydration reaction

In the case of sulfo-aluminous cement-based material, it will be supposed that the two main chemical reactions of hydration of the material are on one hand that associated with the formation of

* Corresponding author.
E-mail address: jean-francois.georgin@insa-lyon.fr (J.F. Georgin).

0008-8846/$ – see front matter © 2010 Elsevier Ltd. All rights reserved.
doi:10.1016/j.cemconres.2010.03.006

ettringite and gibbsite from yeelimite and gypsum and on the other hand that associated with the formation of ettringite from yeelimite, portlandite and gypsum according to the following stoichiometry:

$$C_4A_3\bar{S} + 2C\bar{S}H_2 + 34H \Rightarrow C_6A\bar{S}_3H_{32} + 2AH_3 \quad (1)$$

$$C_4A_3\bar{S} + 8C\bar{S}H_2 + 6CH + 74H \Rightarrow 3C_6A\bar{S}_3H_{32}. \quad (2)$$

Portlandite comes from the hydration of Portland cement which is introduced in the mixture in small quantities (Table 1). In our approach, for the sake of simplicity, as chemical modeling of the Portland hydration is not taking into account, portlandite is supposed to be present in the mixture from the beginning.

The kinetic hydration model proposed in this work is an extension of that proposed in [3]. The reaction advance rates R and R' are of the power law type:

$$R = k\left[C_4A_3\bar{S}\right]^{\alpha}\left[C\bar{S}H_2\right]^{\beta}[H]^{\gamma} \quad (3)$$

$$R' = k'\left[C_4A_3\bar{S}\right]^{\alpha'}\left[C\bar{S}H_2\right]^{\beta'}[CH]^{\gamma'}[H]^{\delta'}. \quad (4)$$

Originality of this formulation lies in the ability to describe the slowing or stopping of the hydration reaction by taking into account the concentration of free water in the early-age material. Indeed, several authors [4] showed in the case of Portland cement-based material that the clinker minerals C_3S, C_2S and C_3A have fundamentally different sensitivities to relative humidity. C_2S hydration is more hampered by decreased relative humidity than C_3S hydration, which again is more hampered than C_3A hydration. In the case of sulfoaluminous cement, in literature, there is no similar work about hydration sensibility to relative humidity. In this work, the accuracy of the proposed chemical model's sensibility to relative humidity is not evaluated. To do that, further investigations are needed in order to link the predicted hydration degree with the measured one for different values of the water to binder cement ratio. The dependence of the hydration kinetics on water concentration taken into account in this approach is of course not really rigorous but has the advantage of providing a given result permitting to generate the porous structure of the material as presented in the following of this paper.

These advance rates define the relation between the product and reagents concentrations because we can also write:

$$R = -\frac{d\left[C_4A_3\bar{S}\right]}{dt} = -\frac{d\left[C\bar{S}H_2\right]}{2dt} = -\frac{d[H]}{34dt} = \frac{d\left[C_6A\bar{S}_3H_{32}\right]}{dt} = \frac{d[AH_3]}{2dt} \quad (5)$$

$$R' = -\frac{d\left[C_4A_3\bar{S}\right]}{dt} = -\frac{d\left[C\bar{S}H_2\right]}{8dt} = -\frac{d[CH]}{6dt} = -\frac{d[H]}{74dt} = \frac{d\left[C_6A\bar{S}_3H_{32}\right]}{3dt}. \quad (6)$$

Characterizing the chemical behavior of the material in modeling point of view consists in determining the parameters (k, α, β, γ) and (k', α', β', δ', γ') which are respectively in Eqs. (3) and (4). The speed coefficient k or k' depends on three characteristic moments used to describe the progression of the mechanisms of dissolution–nucleation.

Table 1
Composition mixtures.

Composition [kg/m^3]	Sulfoaluminate cement	Portland cement	Gypsum	Mineral filler	Water	Fine aggregate
Cement paste	569	65	380.5	254	634	0
Mortar	185	21	124	83	307	1376

In addition to the previous settings, the evolution of the speed coefficients must follow a law of the kind presented in Fig. 1. The number of model parameters to be determined becomes thus 19: k_1, k_2, k_3, θ_1, θ_2, θ_3, α, β, γ and k'_1, k'_2, k'_3, θ'_1, θ'_2, θ'_3, α', β', γ', δ'. An inverse method (the Kalman filter) technique is used based on the experimental measurements of the concentrations evolutions of yeelimite and gypsum in anhydride cement in the case of the hydration of a cement paste (Table 1) with the help of the X-ray diffraction technique (DRX). The degrees of yeelimite and gypsum consumption are then calculated from the following relations:

$$\xi_{\text{yeelimite}} = \frac{\left[C_4A_3\bar{S}\right]^{t=0} - \left[C_4A_3\bar{S}\right]^{t}}{\left[C_4A_3\bar{S}\right]^{t=0}} \quad (7)$$

$$\xi_{\text{gypsum}} = \frac{\left[C\bar{S}H_2\right]^{t=0} - \left[C\bar{S}H_2\right]^{t}}{\left[C\bar{S}H_2\right]^{t=0}}. \quad (8)$$

Values of the chemical modeling parameters are given in Table 2. The fitting of the hydration model was carried out relative to the degree of yeelimite and gypsum consumption as depicted in Fig. 2.

2.2. Chemical shrinkage

Chemical shrinkage, also called «Le Chatelier's contraction» is the consequence of the hydration reaction. Indeed, the sum of the volumes of the reaction products is lower than the sum of the reagent volumes. This difference can be estimated on the basis of the molar volumes of the various chemical substances present, the values of which (Table 3) come from the bibliography [5,6].

The evolution of chemical shrinkage through time can be calculated from the advance rate of the hydration reaction and from the molar contraction derived from the values in Table 3. Indeed, molar contraction is equal to $\chi_{\text{chemical}} = 161.4\ \text{cm}^3$ per mole of yeelimite consumed concerning the first chemical reaction and is equal to $\chi'_{\text{chemical}} = 243.86\ \text{cm}^3$ per mole of yeelimite consumed for the second chemical reaction. The shrinkage kinetics can thus be described according to the following equation relative to the reaction advance rates R and R' and the volume fraction of binder:

$$\frac{dV_{\text{hydrat}}}{dt} = -\left(R\chi_{\text{chemical}} + R'\chi'_{\text{chemical}}\right)\left(1 - \frac{m_{\text{aggregate}}}{\rho_{\text{aggregate}}}\right). \quad (9)$$

$m_{\text{aggregate}}$ is the aggregate mass per unit of volume of mortar (Table 1) and $\rho_{\text{aggregate}} = 2600\ \text{kg m}^{-3}$ is the aggregate density.

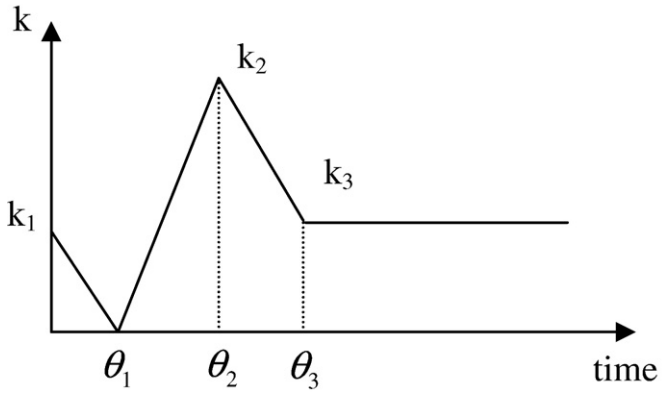

Fig. 1. Evolution of the chemical velocity coefficient k versus time.

Table 2
Chemical modeling parameters.

k_1	2.69e−015	k'_1	1.18e−016
k_2	1.93e−013	k'_2	2.54e−016
k_3	4.41e−014	k'_3	2.70e−016
θ_1	48,843 s	θ'_1	35,512.6 s
θ_2	49,839.8 s	θ'_2	45,899.4 s
θ_3	93,580.8 s	θ'_3	85,842.3 s
α	0.931	α'	1.000
β	0.944	β'	0.910
γ	1.398	γ'	1.059
		δ'	1.123

The comparison between the measured chemical shrinkage kinetics on mortar (Table 1) and that predicted by modeling is shown in Fig. 3. On the basis of the theoretical values of molar volumes and the aggregate volume fraction, this result seems to confirm that the chemical shrinkage of the material responsible for creating internal voids seems to be well correlated with the degree of hydration.

2.3. Porosity

The porosity corresponds by definition to the volume fraction of the empty spaces in the porous network. The total porosity ϕ evolution kinetics is linked to the water consumed by hydration and the chemical contraction of the products of the reaction. Macroscopically, the porosity evolution speed can be expressed in the following form:

$$\frac{d\phi}{dt} = \left(R\chi_{\text{chemical}} + R'\chi'_{\text{chemical}} - R\chi_{\text{hydration}} - R'\chi'_{\text{hydration}}\right)\left(1 - \frac{m_s}{\rho_{\text{aggregate}}}\right). \quad (10)$$

The initial total porosity is given by the volume of initial water in the blend: $\phi^0 = \frac{m^0_{\text{water}}}{\rho_{\text{water}}}$ and by the air entrained which is estimated to $\phi^{\text{air}} = 3\%$.

The terms $\chi_{\text{hydration}}$ and $\chi'_{\text{hydration}}$ correspond to the volumes of water chemically bound by the degree of reaction advance. They are calculated from both the stoichiometry of the chemical reactions and the molar volume of the water, here:

$$\chi_{\text{hydration}} = 34{*}18 = 612\,\text{cm}^3\,\text{mol}^{-1} \quad (11)$$

$$\chi'_{\text{hydration}} = 74{*}18 = 1332\,\text{cm}^3\,\text{mol}^{-1}. \quad (12)$$

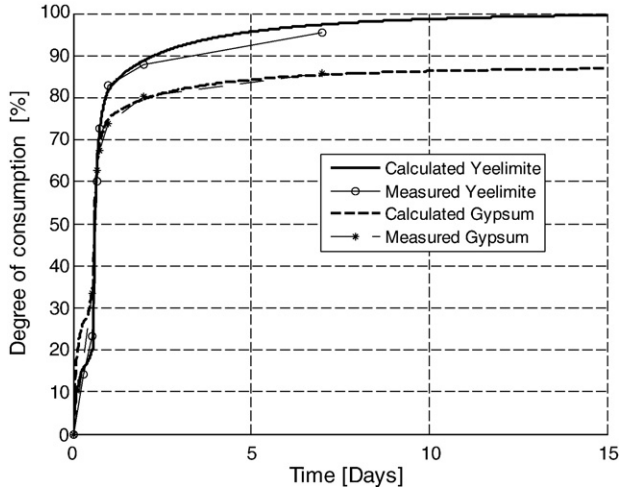

Fig. 2. Results of the modeling fitting in terms of yeelimite and gypsum consumptions (cement paste).

Table 3
Molar volume given in [5,6].

	Notation	Molar volume [cm^3 mol^{-1}]
Yeelimite	$C_4A_3\bar{S}$	234.00
Gypsum	$C\bar{S}H_2$	74.20
Water	H	18.00
Ettringite	$C_6A\bar{S}_3H_{32}$	705.00
Gibbsite	AH_3	64.00
Portlandite	CH	33.21

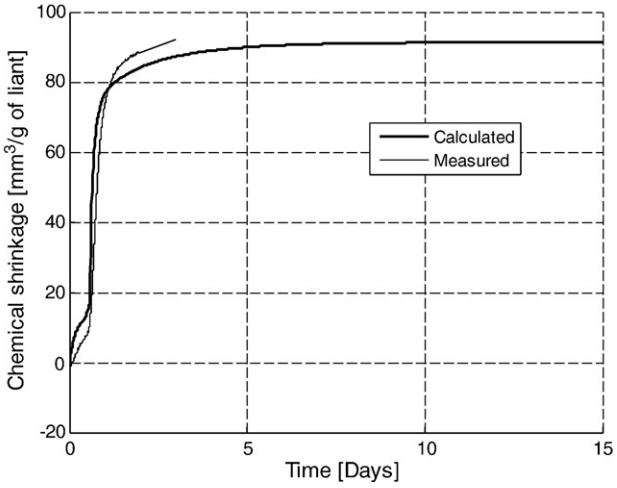

Fig. 3. Measured and calculated comparison of the chemical shrinkage (mortar).

Fig. 4 presents the evolution of the porosity calculated with the preceding equations. Similarly, the porosity in mortar specimen kept in endogenous configuration measured by mercury intrusion porosimetry after 19 h, 24 h and 14 days is given. The prediction of porosity is of good quality. Besides, this modeling of porosity evolution kinetics has the advantage that it can decompose into two essential sources making the porous area inside the cement-based material. Proposition is to consider that a first component of the total porosity is linked to the space area of the inner hydrates products, the finer porosity ϕ_{chemical}, which is supposed in our approach to be the result of the chemical contraction of hydrates, and a cruder form of porosity $\phi_{\text{capillary}}$ which is induced by water not chemically bound and which subsists in the material.

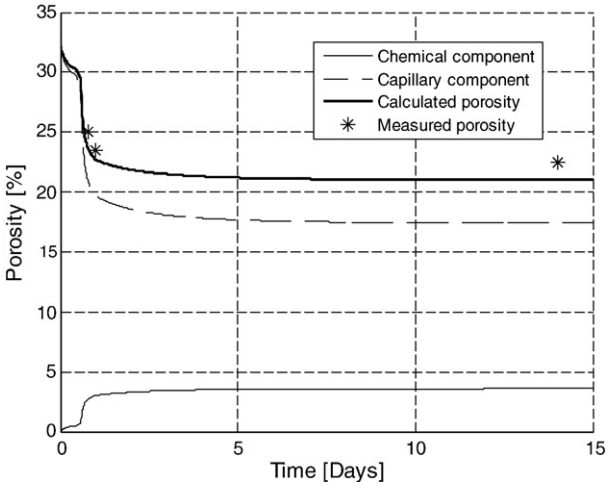

Fig. 4. Calculated and measured porosity comparison (mortar).

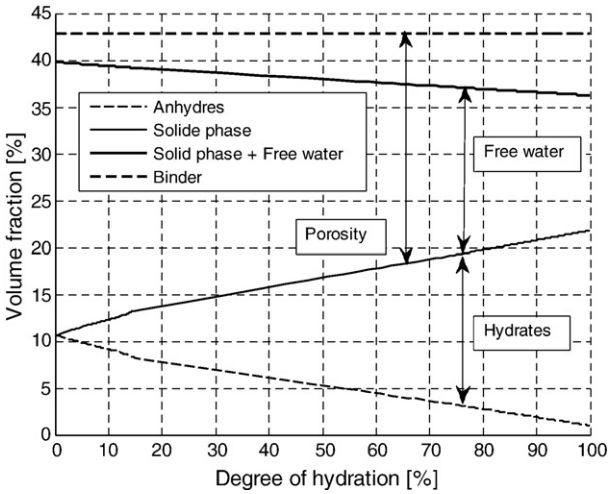

Fig. 5. Evolution of volume fractions versus the degree of hydration in the binder (mortar).

Thus the following decomposition is obtained:

$$\phi_{\text{chemical}} = \left(1-\frac{m_{\text{aggregate}}}{\rho_{\text{aggregate}}}\right)\int\left(R\chi_{\text{chemical}} + R'\chi'_{\text{chemical}}\right)dt \tag{13}$$

$$\phi_{\text{capillary}} = \phi^{\text{air}} + \frac{m^0_{\text{water}}}{\rho_{\text{water}}} - \left(1-\frac{m_{\text{aggregate}}}{\rho_{\text{aggregate}}}\right)\int\left(R\chi_{\text{hydration}} + R'\chi'_{\text{hydration}}\right)dt. \tag{14}$$

Fig. 5 shows evolutions of the calculated volume fraction of anhydres, hydrates, free water and porosity in the case of endogenous configuration versus the degree of hydration $\xi_{\text{yeelimite}}$. The volume fraction of the solid phase increases with the increasing degree of hydration. Self-desiccation is put in light by the increasing difference between the total binder and the (solid phase + free water) volume fraction. The initial difference is linked to the air entrained ϕ^{air}.

2.4. Pore-size distribution modeling

In a non saturated situation and for a given relative humidity h, the meniscus of radius R_m constitutes the frontier between the volume fraction $(V_{\text{porosity}} - V_{\text{liquid}})$ of the porous network occupied by the gas phase and the volume fraction V_{liquid} saturated with liquid water. The corresponding capillary pressure p_c is linked to the radius R_m of the meniscus himself linked to relative humidity h following the Kelvin Laplace equation:

$$p_c = \frac{2\gamma}{R_m}\cos(\theta) = -\rho_{\ell}\frac{RT}{M_v}\ln(h) \tag{15}$$

where the water surface tension $\gamma = 0.0728\ \text{N m}^{-1}$, the water contact angle $\theta = 0°$, the constant of perfect gas $R = 8.314\ \text{J mol}^{-1}\ \text{K}$, the water density $\rho_{\ell} = 1000\ \text{kg m}^{-3}$, the molar mass of vapour $M_v = 0.01802\ \text{kg mol}^{-1}$ and the absolute temperature $T = 293.15\ \text{K}$ are well-known and are remembered in [7].

The R_p radius pores concerned by this meniscus are then determined by the thickness δ of the layer of water adsorbed as depicted in Fig. 6 following the equation:

$$R_p = R_m + \delta. \tag{16}$$

The volume fraction of water adsorbed V_{adsorbed} on the surfaces of the porous network occupied by the gaseous phase is taken into account in the volumic result by way of the relation proposed by Bentz et al. [8] linking the thickness of water δ adsorbed in nm to the given relative humidity h:

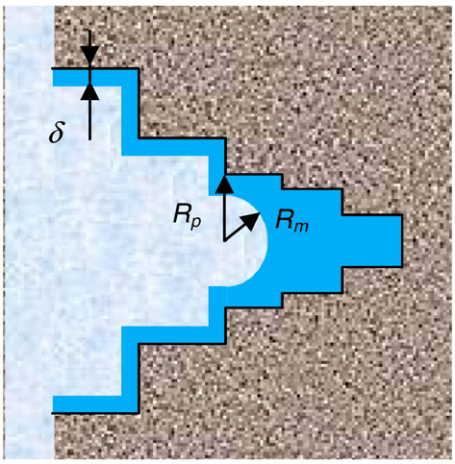

Fig. 6. Simplified scheme of the porosity.

$$\delta(h) = 0.395 - 0.189\ln(-\ln(h)). \tag{17}$$

The degree of saturation S_{ℓ} can thus be determined:

$$S_{\ell} = \frac{V_{\text{liquid}} + V_{\text{adsorbed}}}{V_{\text{porosity}}}. \tag{18}$$

The values of V_{liquid} and V_{porosity} are determined on the cumulated pore-size distribution curve, for a given pore radius R_p as indicated in Fig. 7. The cumulated pore-size distribution curve may be obtained experimentally by mercury intrusion porosimetry measurement technique. The volume fraction of water adsorbed V_{adsorbed} is evaluated from the following expression:

$$V_{\text{adsorbed}} = \int_{R_p}^{\infty}\left[\pi r^2 - \pi(r-\delta)^2\right]dl = \int_{R_p}^{\infty}\left[1-\left(1-\frac{\delta}{r}\right)^2\right]\frac{dV}{d\log r}d\log r \tag{19}$$

where we assume a geometrical structure of the porous network which is approximated with a successive piling up of cylindrical tubes of diminishing radius as schematized in Fig. 6. The fact that lower-radius pores can open onto higher radius pores is not considered.

Knowing the degree of saturation versus capillary pressure relationship for a given relative humidity h, the treatment of the whole cumulated pore-size distribution curve thus leads to determining the capillary pressure curve $p_c(S_{\ell})$.

At an early age, the idea is to describe the pore-size distribution curve $V = f(R_p, \xi_{\text{yeelimite}})$ which depends then on the degree of

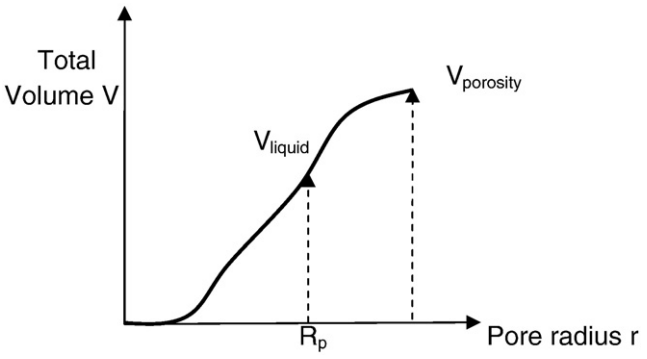

Fig. 7. Typical cumulated pore-size distribution curve.

hydration $\xi_{yeelimite}$ with a mathematical function in order to provide p_c (S_ℓ, ξ) curves. As we can observe clearly that the pore-size distribution is generally broken down into two major pore families (Fig. 8a), the first proposal in this work is to consider that the volume fraction of the pores family in the range around radius equal 10^{-2} μm is equal to the porosity defined previously as fine porosity with $V^1_{chemical}(r=\infty, \xi_{yeelimite}) = \phi_{chemical}$ (Fig. 8b). The second proposal is to consider that the volume fraction of the larger pores family is the volume fraction of water not consumed by hydration, supposed to constitute the macro-porosity which is separated into two components with $V^2_{capillary}(r=\infty, \xi_{yeelimite}) = (1-\omega)\phi_{capillary}$ and $V^3_{capillary}(r=\infty, \xi_{yeelimite}) = \omega\phi_{capillary}$ where ω is a weighting scalar (Fig. 8b). Then, volume fraction of the total porosity $V_{porosity}(r, \xi_{yeelimite})$ can be considered as a combination of these components of porosity with the help of this equation (Fig. 8b):

$$V_{porosity}\left(r, \xi_{yeelimite}\right) = \phi_{chemical} H^1_{chemical} + (1-\omega)\phi_{capillary} H^2_{capillary} + \omega\phi_{capillary} H^3_{capillary}. \quad (20)$$

$\phi_{chemical}$ and $\phi_{capillary}$ depend only on the hydration degree $\xi_{yeelimite}$. H^i_j functions define the shape of the pore-size distribution and depend on both the hydration degree $\xi_{yeelimite}$ and on the radius pore r concerned by the meniscus.

The shape of the cumulated pore-size distribution modeling depends on the choice of the mathematical expression H^i_j. This is such that the derived function of H^i_j corresponds to the following Gaussian curve G^i_j:

$$G^i_j(r) = \frac{dH^i_j}{dr}(r) = \frac{1}{\sigma^i_j\sqrt{2\pi}} \exp\left(\frac{\left(\log(r) - \log\left(r^i_j\right)\right)^2}{2\sigma^{i^2}_j}\right). \quad (21)$$

The parameters r^i_j and σ^i_j are identified so that the major pore families coincide with the main families of pores obtained experimentally. They must be dependent on the degree of hydration $\xi_{yeelimite}$ and fitting of the incremental pore size needs to have linear relationships versus $\xi_{yeelimite}$ as:

$$r^i_j\left(\xi_{yeelimite}\right) = a^i_j\left(1 - b^i_j \xi_{yeelimite}\right) \quad (22)$$

$$\sigma^i_j\left(\xi_{yeelimite}\right) = c^i_j\left(1 - d^i_j \xi_{yeelimite}\right). \quad (23)$$

The fitting of the modeling pore-size distribution with the experimental one for 3 time lapses (Fig. 9) leads to determine parameters ω, a^i_j, b^i_j, c^i_j and d^i_j which are given in Table 4. A global evolution kinetics of the cumulated pore-size distribution curve is also obtained through time. A plot of it is given in Fig. 10.

The capillary pressure curve p_c (S_ℓ) is classically determined from the desorption isotherm which translates the water mass sample loses in the drying process. There are nevertheless several experimental disadvantages. On the one hand, each point on the curve is obtained when the core of the sample is in hydric balance with its environment, which takes a long time. On the other hand, within the framework of research on early-age behavior, the curve for each level of hydration must be known, which is experimentally impossible. The formulation of this pore-size distribution model thus enables capillary pressure curves to be generated according to the hydration of the material. The exploitation of the previously presented pore-size distribution model gives the capillary pressure curves p_c (S_ℓ, $\xi_{yeelimite}$) shown in Fig. 11.

2.5. Theoretical evolution of pore pressure

On the basis of the theory of porous environments of Coussy [9], the coupling relation between the mechanical behavior and the hydric state of the material is obtained from the equivalent pore pressure π. This coupling is defined by the constraints and is written in the following form:

$$d\sigma + bd\pi = Kd\varepsilon \quad (24)$$

where σ is the macroscopic constraint and ε is the mechanical deformation. K is the compressibility modulus and b is Biot's coefficient.

The diminution of the degree of saturation S_ℓ leads to the creation of menisci in the porous network which mark the frontier between liquid and gaseous phases in the fluid. In agreement with Coussy et al. [10], the existence of these menisci leads to a balance of surface forces thus:

$$\pi = p^* - U \quad (25)$$

where p^* is the average pressure in the fluid and U is the sum of all the surface energies between liquid and gas, liquid and solid and gas and solid. The total pressure or average pressure of a mixture of ideal gases is equal to the sum of the partial pressures of the individual gases in the mixture as stated by Dalton's law and is written as follows:

$$p^* = S_\ell p_\ell + (1 - S_\ell) p_g. \quad (26)$$

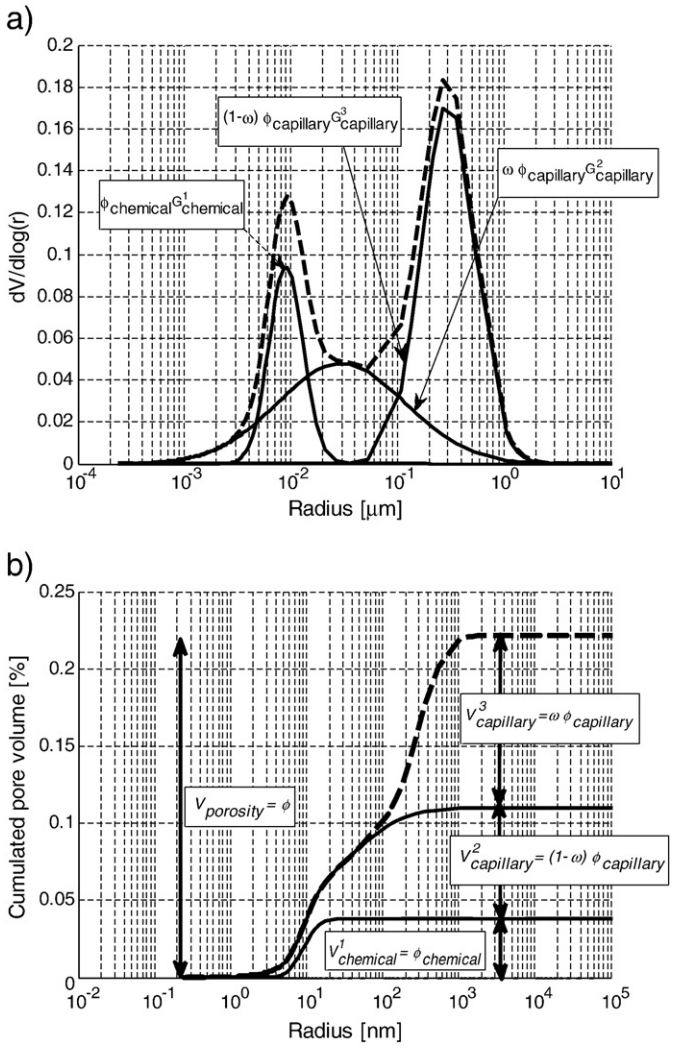

Fig. 8. Incremental a) and cumulated b) pore-size distributions modeling.

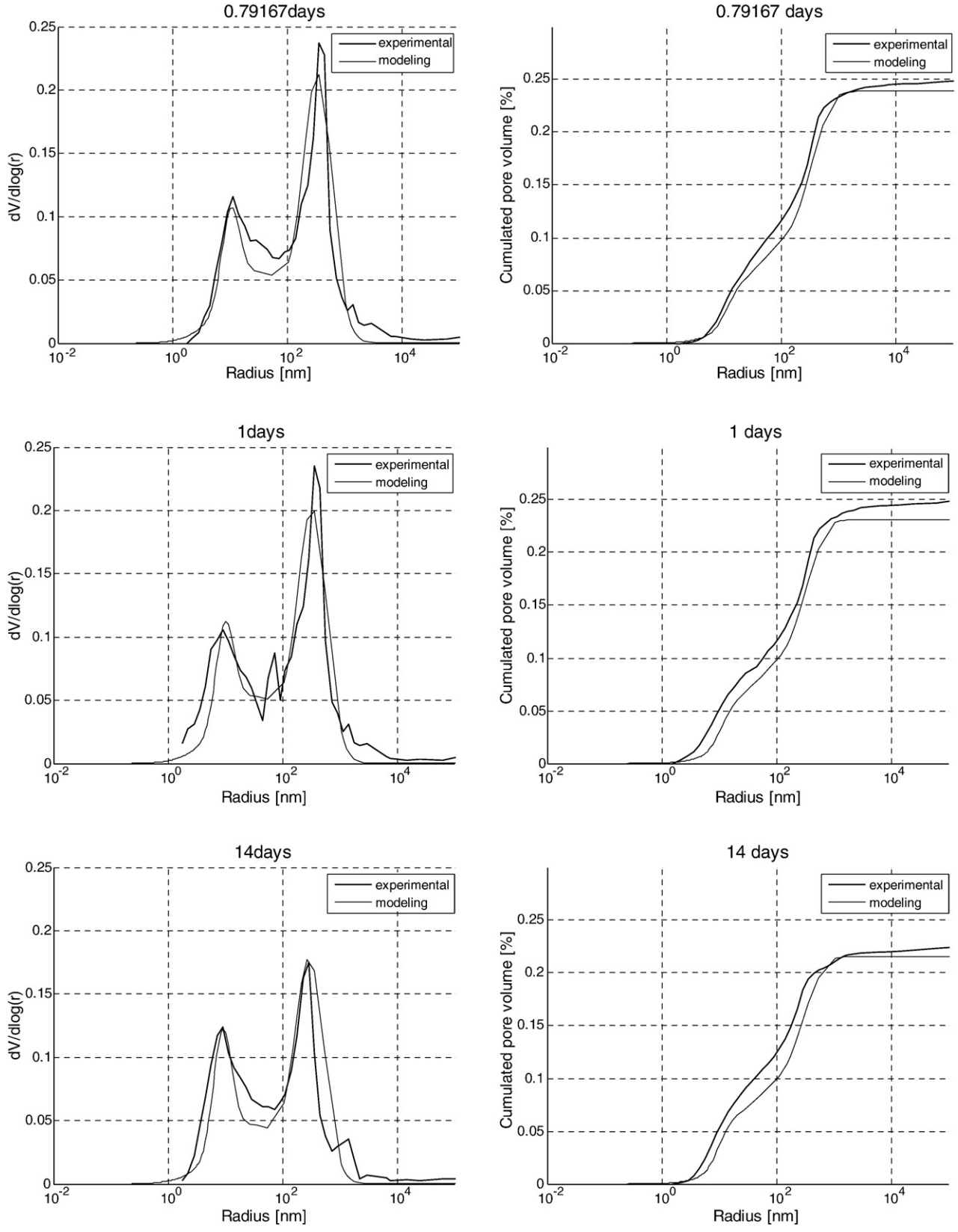

Fig. 9. Calculated and measured pore-size distribution.

Table 4
Pore-size modeling parameters.

ω	3/5
a^1_{chemical}	0.015 μm
b^1_{chemical}	0.4
c^1_{chemical}	0.0016 μm
d^1_{chemical}	0.0
$a^2_{\text{capillary}}$	0.050 μm
$b^2_{\text{capillary}}$	0.4
$c^2_{\text{capillary}}$	0.0006 μm
$d^2_{\text{capillary}}$	0.0
$a^3_{\text{capillary}}$	0.500 μm
$b^3_{\text{capillary}}$	0.4
$c^3_{\text{capillary}}$	0.0003 μm
$d^3_{\text{capillary}}$	0.25

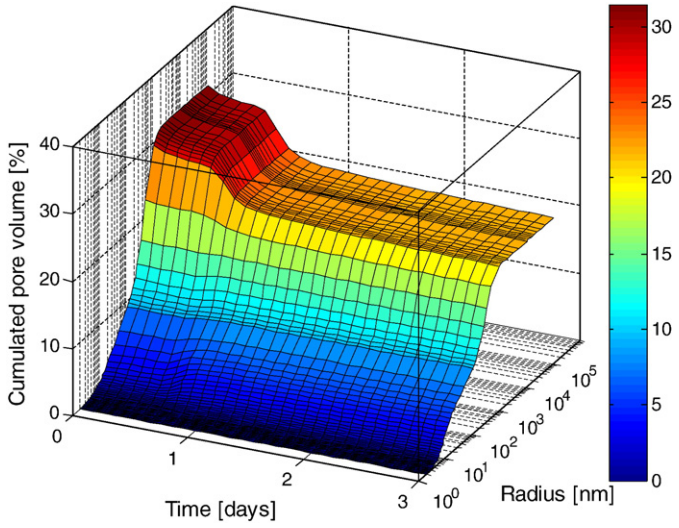

Fig. 10. Global cumulated pore-size distribution modeling.

The sum of surface energies is defined by the area under the capillary pressure curve p_c (S_ℓ):

$$U(S_\ell) = \int_{S_\ell}^{1} p_c(S_\ell) dS_\ell. \tag{27}$$

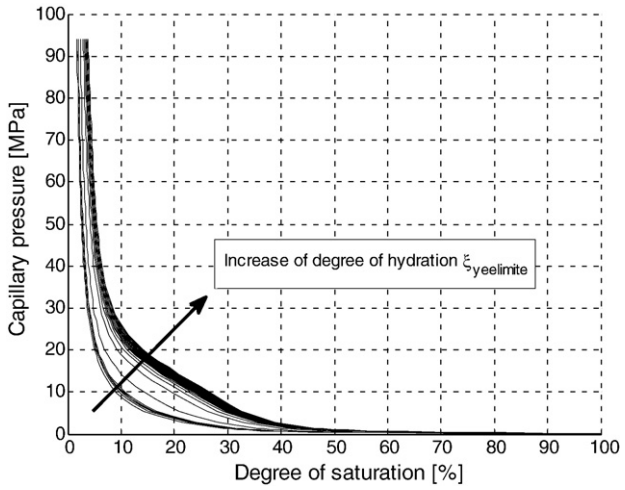

Fig. 11. Calculated p_c (S_ℓ, $\xi_{yeelimite}$) curves with the increase of the degree of saturation.

Thus, the equivalent pore pressure differential is written:

$$d\pi = -S_\ell dp_c + dp_g. \tag{28}$$

Supposing that any gas pressure gradient is rapidly cancelled, the evolution of the equivalent pore pressure is exclusively linked to the capillary pressure and degree of saturation. According to Eq. (24), the effective pore pressure can be defined as follows:

$$dp_{\text{eff}} = -bS_\ell dp_c. \tag{29}$$

For the past century, as that has been summarized comprehensively in [11], many researchers have investigated for the right definition of the Biot's coefficient. Recently, Vlahinic et al. [11] proposed a new definition of this coefficient which essentially needs the experimental characterization of the bulk modulus of the solid constituent k_s. Because these investigations in the case of sulfo-aluminous cement-based material are not yet available in literature, a more classical method was used. Biot's coefficient b can be determined by a homogenization method as presented in [12] where the porosity is included in the solid matrix composed of binder and sand. It can be shown in this case that Biot's coefficient is independent of the compressibility modulus of the solid k_s and the homogenized modulus of compressibility $K = k_{\text{hom}}$. We have:

$$b = 1 - \frac{k_{\text{hom}}}{k_s} = \frac{\phi}{1 - \alpha_s(1-\phi)} \tag{30}$$

with

$$\alpha_s = \frac{3k_s}{3k_s + 4\mu_s} \tag{31}$$

$$k_s = \frac{E_s}{3(1-2\nu_s)} \tag{32}$$

$$\mu_s = \frac{E_s}{2(1+\nu_s)}. \tag{33}$$

It can be shown without difficulty that Biot's coefficient is finally independent of the elasticity modulus E_s of the solid composing the skeleton. Here, Poisson's coefficient ν_S of the solid was taken as constant and equal to 0.2. Then, Biot's coefficient simply depends on porosity ϕ.

Before the setting process begins, the existence of capillary pressure cannot be considered since the skeleton and the porous network are not yet constructed. In modeling terms, the consequence is that the integration of Eq. (29) enabling the evolution kinetics of effective pore pressure to be obtained must be carried out with the percolation point as its lower limit. The percolation point can be deduced at the beginning of setting which separates the moment when the material passes from a fluid-plastic to a solid state with the help of the Vicat apparatus. The measured initial setting time is for the studied mortar around 4 h corresponding to a degree of hydration equal to 10%. The evolution kinetics of calculated capillary pressure and calculated effective pore pressure according to the degree of hydration are shown in Fig. 12 in the case of endogenous configuration.

2.6. Degree of saturation

The deformable skeleton [9] is made up of the solid matrix and the connected porous space filled by fluids which are liquid water (indexed l), water vapour (indexed v) and dry air (indexed a). The displacement of the fluids being considered relative to the skeleton, the elementary volume studied consequently does not contain the same quantity of fluid after skeleton deformation. This is why the

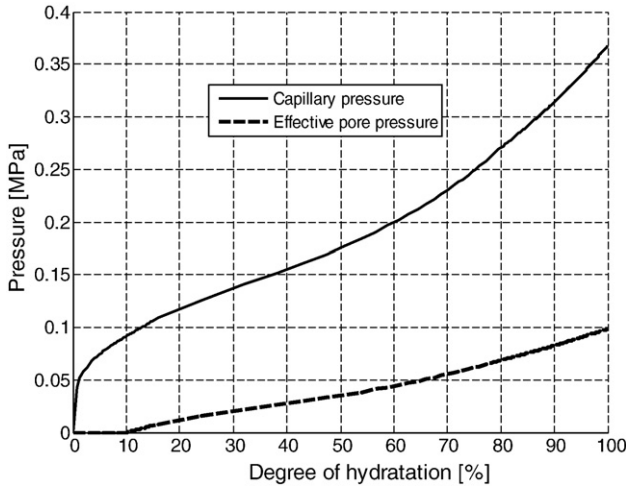

Fig. 12. Pore and capillary pressure evolutions in endogenous configuration (mortar).

initial elementary volume is considered as an open system which exchanges with the outside, a mass ($m_i d\Omega$) of phase i composing the fluid. The principle of mass conservation for each phase is thus expressed as follows:

$$\frac{dm_l}{dt} = div(w_l) - \frac{dm_{l\to v}}{dt} - \frac{dm_{l\xi}}{dt} \tag{34}$$

$$\frac{dm_v}{dt} = div(w_v) + \frac{dm_{l\to v}}{dt} \tag{35}$$

$$\frac{dm_a}{dt} = div(w_a) \tag{36}$$

where w_i is the fluid mass relative flux associated with phase i, and ($m_{l\to v}\, dt d\Omega$) represents the mass of liquid water which is transformed into water vapour in the elementary volume studied.

The mass m_i is linked to the porosity ϕ, the degree of water saturation $S_\swarrow$ and the density ρ_i of the phase i, according to the following expressions:

$$m_\swarrow = \phi \rho_\swarrow S_\swarrow \tag{37}$$

$$m_v = \phi \rho_v (1 - S_\swarrow) \tag{38}$$

$$m_a = \phi \rho_a (1 - S_\swarrow). \tag{39}$$

The mass of hydrated water $m_{l\xi}$ is linked to the advancement of the hydration reactions according to:

$$\frac{dm_{l\xi}}{dt} = -(34R + 74R')M_H \left(1 - \frac{m_{aggregate}}{\rho_{aggregate}}\right) \tag{40}$$

where $M_H = 18\ g\ mol^{-1}$ is the mass molar of water.

Supposing that the transport mechanisms are perfectly dissociated, the liquid phase movement can be described by Darcy's law according to the expression of the flow:

$$w_\swarrow = -\rho_\swarrow \frac{k}{\eta_\swarrow} k_{r\swarrow}(S_\swarrow) grad(p_\swarrow) \tag{41}$$

where k is the intrinsic permeability, $k_{r\swarrow}$ is the permeability relative to water and $\eta_\swarrow$ is the dynamic viscosity of the water.

The transport of the water vapour through the dry air can be described both by Darcy's law and Fick's law. The water vapour flow can be written as follows:

$$w_v = -\rho_v \frac{k}{\eta_g} k_{rv}(S_\swarrow) grad\left(p_g\right) - f(\phi, S_\swarrow) \frac{D_{va}(T)}{p_g C_v} grad(C_v) \tag{42}$$

where $\frac{D_{va}(T)}{p_g}$ is the diffusion coefficient of water vapour or dry air in wet air ($cm^2\ s^{-1}$), $f(\phi, S_\swarrow)$ is the resistance factor accounting for both the tortuosity effect and the reduction of space offered to the diffusion of gaseous constituents, and C_v is the molar density of water vapour.

If the conservation of the mass of liquid water and water vapour is considered, the following equation is obtained:

$$\frac{d(\phi \rho_l S_l + \phi \rho_v (1 - S_l))}{dt} - div(w_l + w_v) = -\frac{dm_{\swarrow\xi}}{dt}. \tag{43}$$

A numerical study was carried out by Mainguy [13] in which all the means of transport mentioned before (liquid water and water vapour convection, and diffusion of vapour in air) are considered. In the case of materials with a cement matrix with an intrinsic permeability close to 10^{-18} m^2, the low dynamic viscosity value of a gas compared to the dynamic viscosity of a liquid enables water vapour transport in a convective form to be left aside considering the relatively long time scale required for drying. Besides, the numerical results also show that, contrary to the constant gas pressure hypothesis too often advanced, the gas phase can be subjected to very high excess pressure. However, the homogeneity of vapour concentration being rapidly observed in a material of low permeability, this enables the Fickean transfer of water vapour to be left aside. Lastly, considering that the density of water vapour is much lower than that of liquid water, the Eq. (43) can be simplified and re-written in the following form:

$$\frac{d(\phi \rho_l S_l)}{dt} - div(w_l) = \frac{dm_{\swarrow\xi}}{dt}. \tag{44}$$

The incompressibility of water, the capillary definition ($p_c = p_g - p_\swarrow$) and the Eqs. (41) and (44) lead to the following relation:

$$\phi \frac{dS_l}{dt} - div\left(\frac{k}{\eta_l} k_{rl}(S_l) grad(p_c)\right) = \frac{1}{\rho_l} \frac{dm_{\swarrow\xi}}{dt} - S_\swarrow \frac{d\phi}{dt}. \tag{45}$$

3. Measuring pore pressure

The test developed consists in measuring from the pouring stage the variations in pore pressure in the material in endogenous configuration during hydration. The measurements are carried out thanks to a set-up similar to that used to measure interstitial pressure in floors [14–16]. A fine ceramic porous stone is plunged into the fresh material. It ensures the continuity between the water in the material and the water in the sensor chamber. The perfect saturation of the ceramic stone by deaerated water is an essential condition for the correct functioning of the tensiometer [17].

The sample is poured up to 5 cm thick into a recipient 6 cm in height and 8 cm in diameter (Fig. 13). Distilled and deaerated water is then used to fill the whole glass device: the lower part of the pressure sensor, the capillary tube and the porous ceramic stone. The saturated ceramic stone, 2 cm long, is then immerged directly in the sample. It is systematically placed at the same depth in the material: 1.5 cm from the bottom of the mold and 1.5 cm from the surface.

Lastly, oil is poured 1 cm thick on the surface of the sample so that the material is in perfectly endogenous condition.

Before setting begins, that is, when the material is still fluid and shows no rigidity, hydration of the material leads to a fall in volume which is relative to the chemical contraction. The water in the

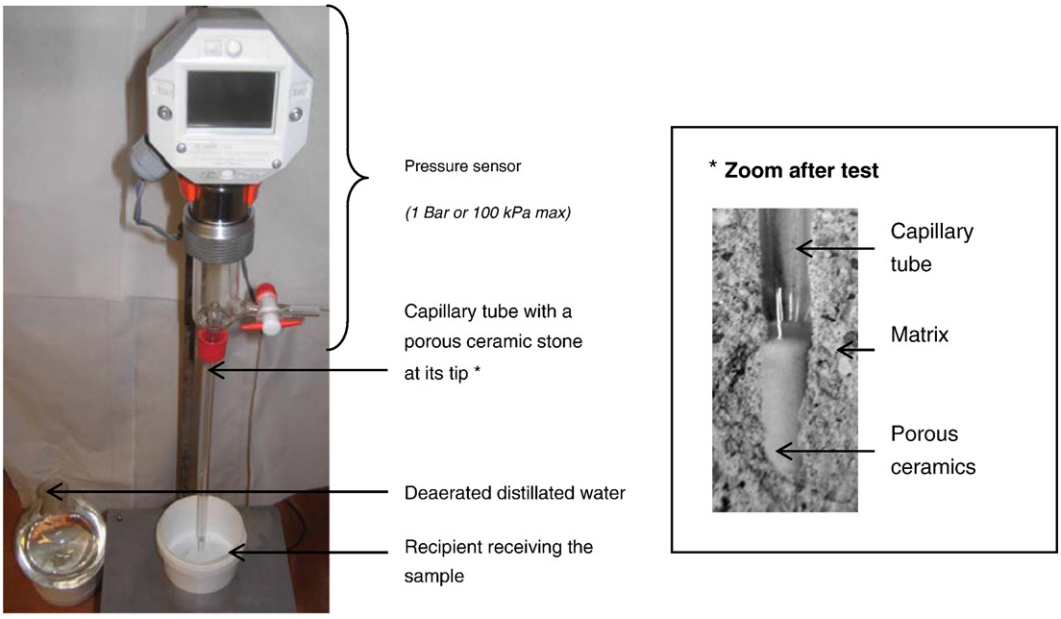

Fig. 13. Experimental pore pressure measuring device.

sensor tank compensates for this created volume. A slight depression is then measured between 4 and 12.5 h (Fig. 14). Then when setting has begun, that is, when the porous structure is formed, the depression measured by the sensor is also due to the cavitation mechanism in the material, hence the sudden increase in depression between 12.5 and 16 h. Finally, when the desaturation kinetics is stabilized because the hydration reaction is practically over, the depression is also stabilized.

Fig. 14 presents also the comparison between the measured depression evolution and that calculated relative to time. The close correspondence until 0.06 MPa between experiment and calculation hints at interesting horizons in predicting shrinkage at an early age in materials with a cement matrix. But a difference occurs nevertheless after this level of pressure. An experimental reason may be behind this discrepancy. Indeed, the saturated ceramic stone supplies certainly water inside the material on a distance of a magnitude equivalent to the size of the sensor, which leads to underestimate the theoretical local depression. In reality, that means that the material situated near the ceramic stone is not in perfectly endogenous condition but is in drained condition. As already presented in [14–16], this technique is accuracy for detecting only the beginning of self-desiccation. But nevertheless, this relatively good adequacy demonstrates that the definition of the equivalent pore pressure is reliable unlike the direct comparison between measured pore pressure and capillary pressure which is equal to 0.4 MPa when hydration is completed (Fig. 12).

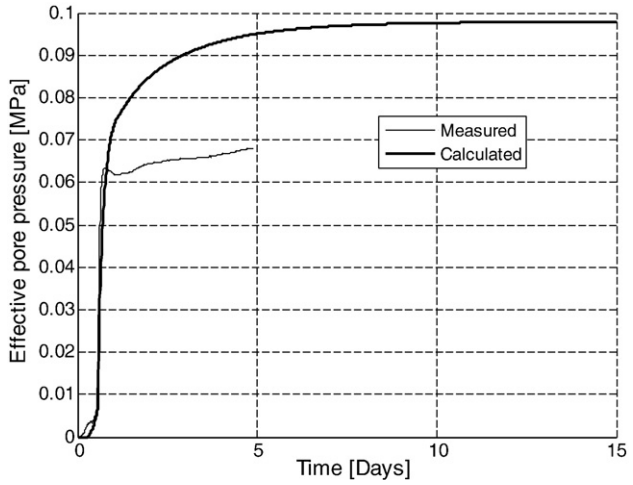

Fig. 14. Evolution kinetics of effective pore pressure in endogenous configuration (mortar).

4. Measuring mass loss in drying configuration

From the mechanisms presented above, it is now opportune to estimate the influence of drying on the hydration of porous material. The considerable drop in the degree of saturation in zones close to the exchange surface can have non negligible consequences on the evolution of porosity and porous distribution. Besides, lower values for the degree of saturation than in an endogenous situation is synonymous with greater pore pressure in the material.

For this estimation, self-leveling screed 3 cm thick subjected to 50% ambient humidity is considered (Fig. 15). More particularly, it is supposed that the drying of the upper face of the porous environment begins as soon as the environment exists, that is, as soon as setting begins. The screed is furthermore considered to have been poured into an impermeable mold, which implies that the flow of water on the lower face and sides is non-existent.

In the Eq. (45), values of the intrinsic permeability k and of the permeability relative to water $k_{r\ell}$ are unknown. It is proposed in literature that the relative water permeability could be described by the Mualem's model [18]:

$$k_{r\ell} = \sqrt{S_\ell}\left[1-\left(1-S_\ell^{\frac{1}{m}}\right)^m\right]^2. \quad (46)$$

Concerning the intrinsic permeability k, experimental results given in [19] exhibit data showing a linear relation between the intrinsic permeability or gas permeability and the total porosity. It is evident that permeability doesn't depend only on porosity but also on tortuosity, specific surface, pore-size distribution and connectivity of pores. But for simplicity, we consider in this work a linear relation between intrinsic permeability k and porosity ϕ:

$$k = a\phi + b. \quad (47)$$

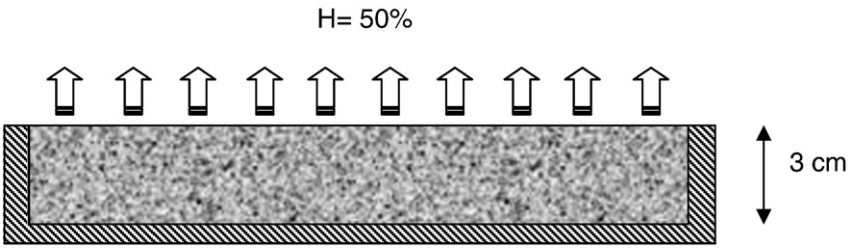

Fig. 15. Experimental scheme of screed subjected to drying.

The hydric flow on the surface of hydric exchange is taken to be proportional to the degree of saturation differential between the boundary layer and the inside of the material:

$$w_{\ell} = \beta\left(S_{\ell} - S_{\ell}^{\text{ext}}\right). \tag{48}$$

The degree of saturation S_{ℓ}^{ext} in the boundary layer is calculated through the curve:

$$p_c\left(S_{\ell}^{\text{ext}}, \xi_{\text{yeelimite}}\right) = -\rho_{\ell}\frac{RT}{M_v}\ln\left(h^{\text{ext}}\right) \tag{49}$$

where the relative humidity h^{ext} outside the screed is equal to 50% and the degree of hydration $\xi_{\text{yeelimite}}$ in the boundary layer is given with the chemical modeling previously presented.

With a view to estimating the impact of the hydric transfer on the development of the material structure, parameters a, b and β are chosen in order to have the best modeling prediction of the loss in water mass (Fig. 16) of the screed. Parameters are given in Table 5. A slight difference still exists and can be induced by the effect of temperature which accelerates the drying mechanism. Elevation of temperature comes from the heat of hydration. Experimental investigations have shown that the temperature elevation at half-way through the thickness is higher in the case of endogenous configuration (5 °C) than in drying configuration (2 °C).

The simulation results presented in Fig. 17 show that the hydration value close to the exchange surface is slightly lower than that situated in the core of the screed. After 14 days, the yeelimite is only 95% hydrated while close to the intrados, it is almost 100% hydrated. Unlike Portland cement [4], the influence of the degree of saturation on hydration seems less marked but this observation is based solely on modeling results and requires experimental verification. The influence of drying is nevertheless clearly visible in Fig. 18 where the degree of saturation through time and in relation to the geometrical position in the thickness of the screed is shown. A few hours after setting begins (12 h), the degree of saturation falls to about 40% on the outer layer while throughout a considerable part of the thickness, the porous environment remains 80% saturated.

The existence of two mechanisms leading to the desaturation of porous networks can be clearly observed in Fig. 18. The first, which is relative to the hydration of the material, is visible in the intrados, while the second, which is linked to the drying process, is visible throughout the total thickness of the screed later in time. The consequences concerning the evolution kinetics of total porosity are similar to what has been identified concerning the degree of hydration of the material. The surface layer of the screed presents after 14 days a relatively higher porosity of about 21.5% and a porosity of 21% throughout the rest of the thickness of the screed as shown in Fig. 19. The difference is more pronounced at an early age but remains nevertheless small. It can thus be deduced that the thickness of the surface layer in which the drying interacts with the hydration of the material is about 5 mm, with the rest not being affected. This numerical result is in accordance with the weak influence of drying on porosity experimentally observed. The porosity measured by mercury intrusion porosimetry reveals almost no noticeable difference whatever the position of the mortar sample studied in the

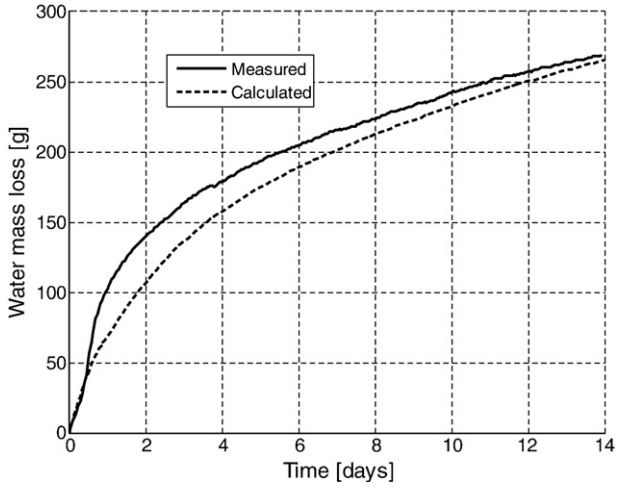

Fig. 16. Measured and calculated screed water mass loss comparison (mortar).

Table 5
Intrinsic permeability, permeability relative to water and hydric flow law parameters.

m	0.49
a	$\frac{580}{3}10^{-19}$
b	$-\frac{113}{3}10^{-19}$
β	10^{-8}

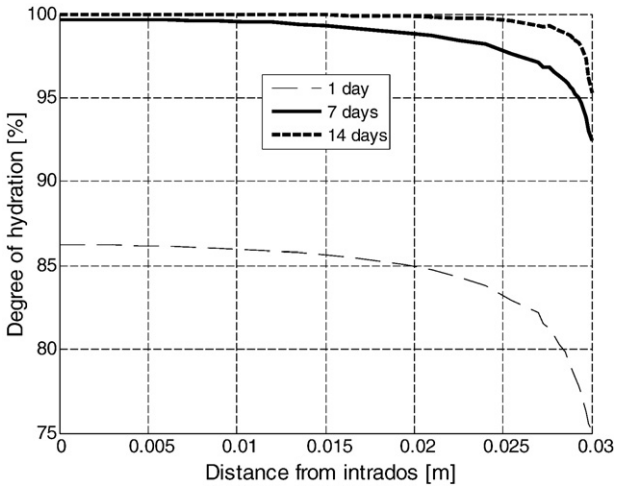

Fig. 17. Evolution in the degree of hydration in the thickness of the screed.

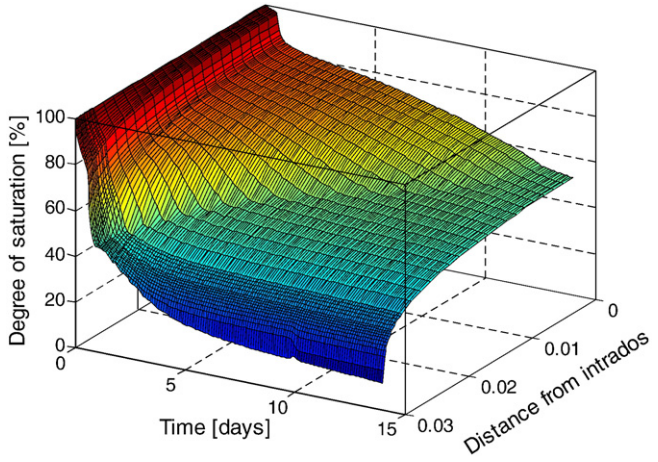

Fig. 18. Evolution in the degree of saturation in the thickness of the screed versus time.

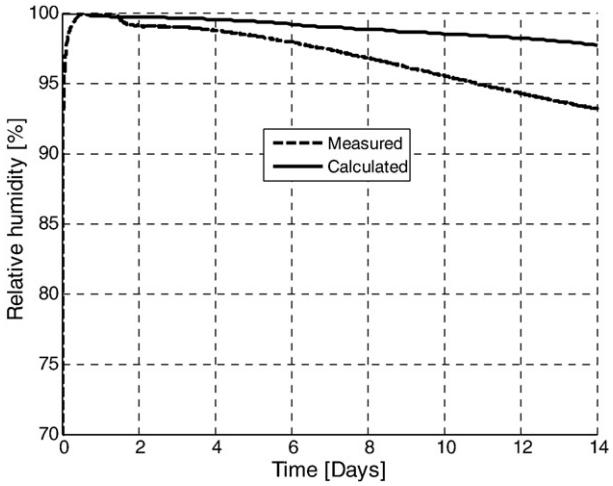

Fig. 20. (RH) at half-way through the thickness versus time.

thickness of the screed. Nevertheless, with a view to validating the representativity of the hydric transfer model, the relative humidities decreasing at half-way through the thickness (Fig. 20) given by the model and that measured with Rotronic hygroclip2 SC05 probe are compared. Modeling overestimates the value of the measured (RH). This result seems to put in fault condition the developed modeling. But further works are necessary to check if the humidity measurement with a probe of diameter of several mm is representative of moisture actually present in pores with diameters less than 1000 times. Another aspect cited in [7] is not considered in this work and also not clearly observed in terms of (RH) measurement. An initial (RH) drop can be attributed to dissolved salts in the pore fluid.

Knowing the characteristics of the porous structure and the degree of saturation throughout the thickness of the screed relative to time enables the distribution of the effective pore pressure in the material to be calculated. The evolution of the effective pore pressure in the thickness through time is shown in Fig. 21. It can be observed that it evolves from a value of a few hundredths of MPa (0.1 MPa) in an endogenous configuration to a few MPa in a drying situation (2.5 MPa). Supposing that the material is only elastic from the start of the setting process, after 14 days, the elasticity module being of the order of 10 GPa, that leads to a shrinkage deformation of 250 μ. The values measured are generally higher than this. In fact, the material is certainly viscoplastic and in this case the history of both pore pressure and elastic modulus since the setting began must be integrated to obtain shrinkage.

5. Conclusions

Knowledge of early-age behavior of materials with a cement matrix is an important factor for the improvement of their durability. Indeed, the dimensional variations they are subjected to can cause high constraints in the first days leading to cracking. With a view to understanding in more detail the certain mechanisms responsible for shrinkage deformation, a modeling tool has been presented and calibrated both in endogenous configuration and in a drying situation. It is based on a description of the hydration reaction and on a modeling of the porous distribution from which the evolution kinetics of capillary pressure relative to the degree of saturation is constructed. Several calculated values such as chemical shrinkage, effective pore pressure (endogenous), relative humidity (during drying) and mass loss have been compared to measured values. The quality of the results obtained proves the potential of this numerical approach in characterizing in a general way the material levers responsible for early-age volumic variations. Thermic behavior must be taken into account in the analysis, but that poses no major problem for the mechanisms to be modeled, as only the thermic characteristics need to be identified. The extension of the experiments used in this work to the measurement of temperatures is one of the perspectives. Similarly, the consequences of effective pore pressure on macroscopic deformations will be studied.

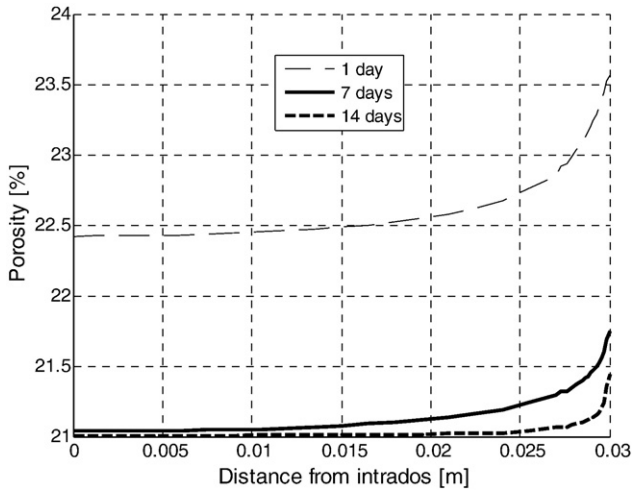

Fig. 19. Evolution in the porosity in the thickness of the screed.

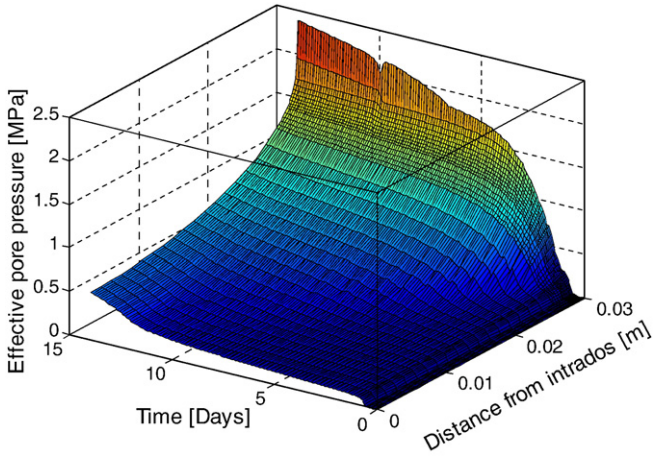

Fig. 21. Evolution in effective pore pressure in the thickness of the screed versus time.

References

[1] T. Kuryatnyk, et al., Improvement of calcium sulphate water resistance by addition of calcium sulphoaluminate clinker, Materials Letters 62 (2008) 3713–3715.
[2] J.F. Georgin, et al., Development of self-leveling screed based on calcium sulfoaluminate cement: modelling of curling due to drying, Cement and Concrete Composite 30 (2008) 769–778.
[3] V.G. Papadakis, C.G. Vayenas, et M.N. Fardis, Physical and chemical characteristics affecting the durability of concrete, ACI Materials Journal 8 (1991) 186–196.
[4] O.M. Jensen, P.F. Hansen, E.E. Lachowski, F.P. Glasser, Clinker mineral hydration at reduced relative humidities, Cement and Concrete Research 29 (1999) 1505–1512.
[5] E. Gartner, Industrially interesting approaches to "low-CO_2" cements, Cement and Concrete Research. 34 (2004) 1489–1498.
[6] B. Lothenbach, et al., Thermodynamic modelling of the effect of temperature on the hydration and porosity of Portland cement, Cement and Concrete Research 38 (1) (2008) 1–18.
[7] P. Lura, O.M. Jensen, K. Van Breugel, Autegenous shrinkage in high-performance cement paste: an evaluation of basic mechanisms, Cement and Concrete Research 33 (2003) 223–232.
[8] D.P. Bentz, E.J. Garboczi, D.A. Quenard, Modelling drying shrinkage in reconstructed porous materials: application to porous Vycor glass, Modelling Simulation in Material Science Engineering 6 (1998) 211–236.
[9] O. Coussy, Poromechanics. s.l, John Wiley, 2004.
[10] O. Coussy, et al., The equivalent pore pressure and the swelling and shrinkage of cement-based materials, Materials and Structures 37 (2004) 15–20.
[11] I. Vlahinic, H.M. Jennings, J.J. Thomas, A constitutive model for drying of a partially saturated porous material, Mechanics of Materials 41 (2009) 319–328.
[12] O. Bernard, F.J. Ulm, et E. Lemarchand, A multiscale micromechanics-hydration model for the early-age elastic proporties of cement-based materials, Cement and Concrete Research 33 (2003) 1293–1309.
[13] M. Mainguy, Modèles de diffusion non-linéaires en milieux poreux. Applications à la dissolution et au séchage des matériaux cimentaires Ph.D. ENPC, Paris, 1999.
[14] M. Chang Wen, T. Qian, S. Wei, Water consumption of the early-age paste and determination of "time-zero" of self-desiccation shrinkage, Cement and Concrete Research 37 (2007) 1496–1501.
[15] J. Mora-Ruacho, R. Gettu, et A. Aguado, Influence of shrinkage-reducing admixtures on the reduction of plastic shrinkage cracking in concrete, Cement and Concrete Research 39 (2009) 141–146.
[16] V. Slowik, M. Schmidt, R. Fritzsch, Capillary pressure in fresh cement-based materials and identification of the air entry value, Cement and Concrete Composites 30 (2008) 557–565.
[17] F. Soeiro, A. Dessaint, Problèmes posés par la mesure de la pression interstitielle dans les sols, Bulletin of the International Association of Scientific Hydrology 14 (2) (1969) 95–129 [mai].
[18] V. Baroghel-bouny, et al., Characterization and identification of equilibrium and transfer moisture properties for ordinary and high-performance cementitious materials, Cement and Concrete Research 29 (1999) 1225–1238.
[19] Z. Lafhaj, et al., Correlation between porosity, permeability and ultrasonic parameters of mortar with variable water/cement ratio and water content, Cement and Concrete Research 36 (2006) 625–633.